Phonon-drag effect in $FeGa_3$

Maik Wagner-Reetz, Deepa Kasinathan, Walter Schnelle, Raul Cardoso-Gil, Helge Rosner, and Yuri Grin
Max-Planck-Institut für Chemische Physik fester Stoffe, Nöthnitzer Straße 40, 01187 Dresden, Germany

Peter Gille
Ludwigs-Maximilians-Universität München, Theresienstraße 41/II, 80333 München, Germany
(Received 5 May 2014; revised manuscript received 30 October 2014; published 25 November 2014)

The thermoelectric properties of single-crystalline and polycrystalline $FeGa_3$ are systematically investigated over a wide temperature range. At low temperatures, below 20 K, previously not known pronounced peaks in the thermal conductivity (400–800 W K^{-1} m^{-1}) with corresponding maxima in the thermopower (in the order of -16000 μV K^{-1}) were found in single-crystalline samples. Measurements in single crystals along [100] and [001] directions indicate only a slight anisotropy in both the electrical and thermal transports. From susceptibility and heat-capacity measurements, a magnetic or structural phase transition was excluded. Using density functional theory based calculations, we have revisited the electronic structure of $FeGa_3$ and compared the magnetic (including correlations) and nonmagnetic electronic densities of states. Thermopower at fixed carrier concentrations is calculated using semiclassical Boltzmann transport theory, and the calculated results match fairly with our experimental data. The inclusion of strong electron correlations treated in a mean field manner (by LSDA + U) does not improve this comparison, rendering strong correlations as the sole explanation for the low-temperature enhancement unlikely. Eventually, after a careful review, we assign the peaks in the thermopower as a manifestation of the phonon-drag effect, which is supported by thermopower measurements in a magnetic field.

DOI: 10.1103/PhysRevB.90.195206 PACS number(s): 71.28.+d, 72.10.Di, 72.20.My, 72.20.Pa

I. INTRODUCTION

Fe-based semiconductors such as FeSi, $FeSb_2$, and $FeGa_3$ have attracted much attention in the past years due to their interesting physical properties. The hybridization of the transition-metal d orbitals with the main group-metal p orbitals opens up small band gaps of the order of 0.1 eV for FeSi [1], 0.03 eV for $FeSb_2$ [2], and 0.47 eV for $FeGa_3$ [3]. Unusual transport properties and their origins are strongly debated within the community for the past two decades. For example, no clear consensus has been reached on the origin of the extremely high Seebeck coefficient of $-45\,000$ μV K^{-1} around 10 K in $FeSb_2$ single crystals [4]. Until now, the community is split between two main schools of thought, one favoring the presence of strong electron-electron correlations [4–6] while the other proposes phonon-drag mechanism [7,8] as the source for the colossal value of the Seebeck effect. Herein, we present huge thermopower values in the order of $-16\,000$ μV K^{-1} below 20 K for single crystals of $FeGa_3$. The experimental results are based on especially good quality single crystals whose chemical compositions have been carefully checked by x-ray powder diffraction and metallographic analysis. Among the various reasons that can rationalize such a large Seebeck coefficient, the main candidates are (i) the presence of strong electronic correlations, (ii) structural phase transitions, (iii) magnetic phase transitions, and (iv) the interaction of the phonons with the mobile charge carriers via the phonon-drag effect. For example, most of the low-temperature anomalies including the enhanced low-temperature thermopower in FeSi are explained upon including the electronic correlations in realistic many-body calculations [9]. The onset of a magnetic phase transition has been demonstrated as the reason for the presence of distinct features in thermopower in $Mn_{2-x}Cr_xSb$ [10]. Unusual jumps in Seebeck coefficient data have been measured in the parent compound of the Fe-based superconductor LaFeAsO [11], Zn_4Sb_3 [12], and $La_{1.85-x}Nd_xSr_{0.15}CuO_4$ [13], all of which have been explained in terms of structural phase transitions. Recently, the observation of a large negative Seebeck coefficient of -4500 μV K^{-1} at 18 K in single-crystalline $CrSb_2$ has been suggested to emerge from the dominating phonon-drag effect at low temperatures [14].

The intermetallic compound $FeGa_3$ was first found during the systematic studies in the binary system Fe-Ga. The crystal structure was originally ascribed to a noncentrosymmetric structure type $IrIn_3$ [15–17]. On the contrary, a centrosymmetric space group $P4_2/mnm$ was suggested later for the description of the symmetry for the crystal structure of $FeGa_3$ [18]. More recent studies confirmed the centrosymmetric crystal structure and reported the first observation of semiconducting behavior [19]. Thermoelectric properties (TE) at temperatures from 300 to 950 K with negative thermopower values were later determined on polycrystalline samples [20]. The first characterization on $FeGa_3$ single crystals depending on the crystallographic orientation was reported in Ref. [3] but the authors observe the appearance of gallium inclusions of approximately 3% in their samples. $FeGa_3$ was found to be diamagnetic, which was later validated [21]. Presence of an energy gap was established using magnetic susceptibility measurements (0.29–0.45 eV) and as well as by valence band x-ray photoemission spectroscopy ($\leqslant$0.8 eV), while ^{57}Fe Mössbauer spectroscopy revealed the absence of magnetic ordering [21]. Nevertheless, considering the narrow 3d bands, Yin and Pickett [22] explored the option of a magnetically ordered ground state in $FeGa_3$ using total-energy calculations and obtained an antiferromagnetically ordered spin-singlet state upon inclusion of correlation effects. Although no

verifiable experimental evidence for a magnetic transition in $FeGa_3$ exists, muon spin rotation spectra [23] show the existence of a spin-polaron band, which is consistent with the presence of an antiferromagnetic spin-singlet scenario. Photoemission and inverse photoemission spectroscopic experiments [24] have also been performed on single crystals of $FeGa_3$ to probe its electronic structure and provide an estimate for the amount of correlation effects in this material. The measured band dispersions were comparable to calculations based on density functional theory (DFT) which included a Coulomb repulsion parameter $U \approx 3$ eV. Nonetheless, the authors conclude that the correlation effects in $FeGa_3$ are not as significant as in FeSi. Recently, another study on doped $Fe(Ga,Ge)_3$ systems using total-energy calculations reports an itinerant mechanism (i.e., suggesting a minor role of the electron correlations implicitly) for the experimentally observed ferromagnetism in the *n*-type samples [25,26].

In our opinion, the presence/absence of magnetism and/or correlations for the stoichiometric $FeGa_3$ systems is still an open question. Until now, there have been no reports of anomalous transport behavior at low temperatures in $FeGa_3$. We have grown well-defined single crystals of $FeGa_3$ without any Ga inclusions and with a total mass up to 25 g and performed various thermodynamic and transport measurements. Unusually large Seebeck coefficient (in the order of $-16\,000$ μV K^{-1}) and thermal conductivity (400–800 W K^{-1} m^{-1}) below 20 K in single-crystalline samples are observed, which disappears in the polycrystalline specimen with equivalent experimental composition. As mentioned in the opening paragraph, various scenarios could be behind these large Seebeck coefficients and thermal conductivity values. In our work, all the options are explored in detail to rationalize the observed low-temperature feature.

II. METHODS

A. Synthesis and chemical characterization

Single crystals of $FeGa_3$ were grown using the two-phase region $FeGa_3$ + melt of the Fe-Ga phase diagram (flux growth). The elements Fe (powder, 99.99 %, ChemPur) and Ga (shots, 99.9999 %, ChemPur) in the ratio 1:20 were weighed in alumina crucibles and encapsulated in quartz ampoules under argon atmosphere with a pressure of 200 mbar. The mixture was heated at a rate of 5 K min^{-1} up to 1173 K and kept at this temperature for 90 h. After slow cooling from 1173 to 473 K, the crystals were separated from the remaining solidified melt and cleaned with hydrochloric acid to remove any residual gallium from the surface. A rectangular piece, 5.8 mm in length (longest possible rectangular bar), was cut for TE characterization.

The Czochralski method was used as a second technique to grow large single crystals (≈8 mm). Starting from a homogenized melt of composition $Fe_{16.5}Ga_{83.5}$ that had been prepared from Fe (bulk, 99.995 %, Alfa Aesar) and Ga (pellets, 99.9999 %, ChemPur), in a first experiment spontaneous nucleation of $FeGa_3$ occurred at a tapered corundum tip. The general approach has been described in Ref. [27]. In the next crystal growth runs, use was made of [001]-oriented $FeGa_3$ seeds to grow well-defined single crystals of a total mass up to 25 g by slowly crystallizing from a Ga-rich melt using pulling rates as low as 0.1 mm h^{-1} while gradually cooling down the melt according to the changing temperature of the liquid.

For polycrystalline specimens, pieces of the flux-grown crystal were ground to powder and recompacted with the spark plasma sintering (SPS) technique. Using graphite dies, a maximum temperature of 973 K with an uniaxial pressure of 90 MPa was applied for 10 min.

X-ray diffraction data sets of all samples were collected on an Image Plate Guinier Camera Huber G670 [Cu $K\alpha_1$ radiation, $\lambda = 1.540\,56$ Å, $3^\circ \leqslant 2\theta \leqslant 100^\circ$, LaB_6 as internal standard, $a = 4.1569(1)$ Å]. Metallographic investigations were made on plain cross sections after embedding samples in conductive resin (PolyFast, Struers, Denmark) with additional grinding and polishing with micron-sized diamond powders. Wavelength dispersive x-ray spectroscopy (WDXS) investigations of the chemical composition were performed with a Cameca SX 100 spectrometer using FeSi and GaP as standards.

B. Physical measurements

Thermal diffusivity measurements of single-crystalline and polycrystalline samples were performed with the laser flash technique (LFA 427, Netzsch, Germany) in the temperature range from 300 to 773 K. The thermal conductivity κ was derived from the relation $\kappa = \alpha D C_p$, where α is the thermal diffusivity, D is the density, and C_p is the heat capacity, respectively. The density of the obtained pellet determined by the Archimedes method reaches 92% of the theoretical value. Heat-capacity data at high temperatures were determined by differential scanning calorimetry (DSC 8500, Netzsch). The electrical resistivity and the Seebeck coefficient of rectangular bars were determined simultaneously in a commercial ZEM-3 equipment (ULVAC-Riko, Japan) in the temperature range from 300 to 773 K.

For TE properties at low temperatures from 4 to 350 K the thermal conductivity, electrical resistivity, and Seebeck coefficient were measured simultaneously using a commercial system (thermal transport option of a PPMS, Quantum Design, USA). The dependence of thermopower on the magnetic field ($H = 0$ and 9 T) was also measured. Given the fact that the thermal conductivity is very high at low temperatures, we additionally reduced the cross section (thinned) at the middle of the sample as depicted in the inset of Fig. 12 in order to maximize the heat flow, while reducing the temperature jumps at the contacts of the sample to the heater and to the heat sink.

Heat-capacity measurements in zero field (ZF) and in field with $H = 9$ T were carried out using a relaxation method (HC option, PPMS). Magnetic properties were measured on a SQUID magnetometer (MPMS-XL-7, Quantum Design). Zero-field cooling (ZFC, measured in warming) and field-cooling magnetization data were taken in various fields up to $H = 7$ T.

C. Calculational details

The total-energy calculations to obtain the density of states (DOS) and band structure were performed using the

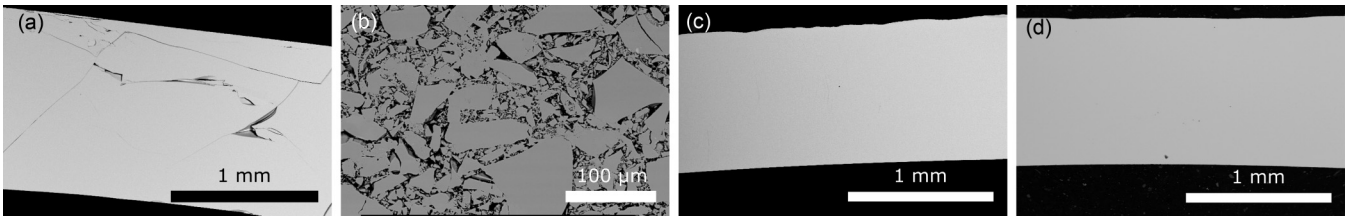

FIG. 1. Secondary electron microstructure pictures of $FeGa_3$ specimens: (a) flux-grown single crystal, (b) polycrystalline specimen after SPS of flux-grown single crystal, (c) single crystal obtained from Czochralski method and oriented along [001], and (d) single crystal obtained from Czochralski method and oriented along [100].

full-potential nonorthogonal local orbital code (FPLO) [28] employing the local density approximation (LDA). The Perdew and Wang [29] exchange-correlation potential was chosen for the scalar relativistic calculations. Additionally, we have explored the possibility of the presence of strong correlations in the Fe $3d$ shell by including an onsite Coulomb repulsion U via the LSDA + U method, applying the "atomic limit" double counting term [also referred to as "fully localized limit" (FLL)]. The projector on the correlated orbitals was defined such that the trace of the occupation number matrices represent the $3d$ gross occupation. The total energies were converged on a dense k mesh with 2176 points ($30 \times 30 \times 30$) for the conventional cell in the irreducible wedge of the Brillouin zone. The transport properties were calculated using the semiclassical Boltzmann transport theory [30–32] within the constant scattering approximation as implemented in BOLTZTRAP [33]. This approximation is based on the assumption that the scattering time τ determining the electrical conductivity does not vary with energy on the scale of $k_B T$. Additionally, no further assumptions are made for the dependence of τ on the temperature. This method has been successfully applied to many narrow-band-gap materials including clathrates, $RuIn_3$ derivatives, as well as other intermetallic compounds and oxides [32,34–37]. Since the evaluation of transport integrals requires an accurate estimation of band velocities, the energy bands are calculated on a fine mesh of 9126 k points in the irreducible wedge of the Brillouin zone.

III. RESULTS AND DISCUSSIONS

A. Chemical characterizations

According to metallographic investigations, the obtained single crystals of $FeGa_3$ via flux-growth and Czochralski methods were free of nonreacted elemental iron or remaining gallium melt (Fig. 1). All x-ray diffraction patterns (see Supplemental Material [38]) of the single- and polycrystalline samples were indexed with the tetragonal $FeGa_3$ structure type (space group $P4_2/mnm$, Fig. 2) without any additional phases. The refined lattice parameters and chemical compositions from WDXS analysis are collected in Table I. The experimental composition for all samples is identical within the typical error limits of the methods. One characteristic feature is the small excess of iron atoms in comparison to the ideal composition. In the paper, thermoelectric and thermodynamic characterizations are performed mainly on single crystals obtained from Czochralski method. The results can be qualitatively inferred for all single-crystalline samples since the chemical composition of all the samples is identical. Any difference in the thermoelectric properties in polycrystalline material in comparison to the single crystals can be attributed to the changes of the microstructure.

B. Thermoelectric properties

The logarithmic plot of the electrical resistivity as a function of temperature is shown in Fig. 3. For all samples, semiconducting behavior is observed. The extrinsic region at low temperatures is characterized by high-resistivity values implying high purity and high crystallinity of our materials.

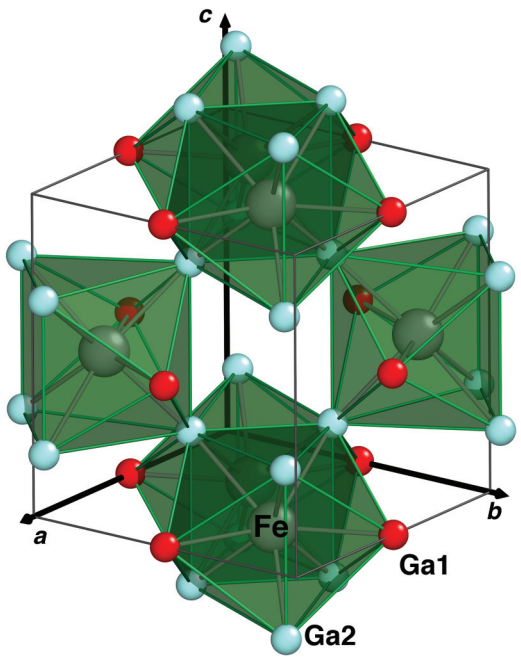

FIG. 2. (Color online) Tetragonal crystal structure of $FeGa_3$ according to Ref. [19]. The large (gray) atoms are Fe, while the smaller (Ga1, red; Ga2, light blue) atoms are Ga [Fe at $4f$ (0.3437,0.3437,0); Ga1 at $4c$ (0,0.5,0); Ga2 at $8j$ (0.1556,0.1556,0.2620)]. The polyhedra surrounding the Fe atom are composed of eight Ga atoms: two nearest-neighbor Ga at a distance of 2.37 Å (Ga1), two next-nearest-neighbor Ga at a distance of 2.39 Å (Ga2), and four third-nearest-neighbor Ga at a distance of 2.50 Å (Ga2). Each Fe atom also has one another Fe atom at a distance of 2.77 Å, forming so-called "dimers" in the (001) plane. The polyhedrons of the iron atoms belonging to the same "dimer" are sharing a common face, while polyhedrons of different "dimers" are corner sharing.

TABLE I. Lattice parameters and experimental compositions from WDXS analysis for single-crystalline and polycrystalline samples of $FeGa_3$.

Experimental composition	a (Å)	c (Å)	V (Å^3)	Remarks
$Fe_{1.023(4)}Ga_{2.98(1)}$	6.2661(1)	6.5597(3)	257.56(1)	Single crystal (flux grown)
$Fe_{1.04(1)}Ga_{2.96(1)}$	6.2663(1)	6.5594(3)	257.56(1)	Polycrystalline SPS specimen (flux grown)
$Fe_{1.018(3)}Ga_{2.982(4)}$	6.2661(2)	6.5596(4)	257.57(1)	Single crystal (Czochralski, oriented along [001])
$Fe_{1.013(3)}Ga_{2.987(4)}$	6.2665(1)	6.5586(2)	257.55(1)	Single crystal (Czochralski, oriented along [100])
$FeGa_3$	6.2628(3)	6.5546(5)	257.09(4)	Ref. [19] Powder (flux grown)
$FeGa_3$	6.262	6.556	257.07	Ref. [3] Single crystal (flux grown)

The flux-grown crystal shows higher resistivity with a terminated saturation range already at 280 K, signifying the lower level of defects and impurities as compared to the other samples. This arises from the fact that the flux-grown single crystals were additionally cleaned with hydrochloric acid which tend to remove extrinsic impurities. From the intrinsic region above 350 K, band gaps were calculated with the Arrhenius law $\rho(T) = \exp(E_g/2k_BT)$, giving a value of 0.50 eV.[1] The experimental data are very well comparable to previously published results (0.47 eV) [3]. A slight anisotropy in $FeGa_3$ is observed below 200 K, with a reduced electrical resistivity in the [100] direction as compared to the [001] direction. A crossover becomes apparent around 250 K, leading to slightly reduced resistivity values in the [001] direction above room temperature.

To determine the carrier concentration, we measured Hall resistivity as a function of magnetic field for selected temperatures along [100] and [001] directions for the current flow. The Hall resistivity data were fit with a linear function for both directions between 10 and 300 K. The determined R_H are negative in the entire temperature range, indicating electrons being the main carriers. The carrier concentration calculated using $n = -1/eR_H$ is plotted in Fig. 4 as a function of temperature (with $e = 1.602 \times 10^{-19}$ C). The carrier concentration does not vary significantly between 100 and 300 K, with room-temperature values: $n^{[001]} = 9.52 \times 10^{19}$ cm^{-3} and $n^{[100]} = 1.03 \times 10^{20}$ cm^{-3}. Below 50 K, we observe an abrupt decrease of n with the lowest value of 4×10^{19} cm^{-3} at 20 K. Such a feature in n is quite unusual and could arise from a low-mobility impurity band close to the conduction band edge, as was shown to be the case for Ge [39]. Recently, another compound where such a feature was observed is the antiferromagnetic semiconductor $CrSb_2$ [14] and the authors determined an occupied low-mobility donor

[1]The unoriented bar-shaped piece, which was cut from the flux-grown crystal, could not be measured at high temperatures, owing to its short length for the unoriented crystal, a band gap of 0.38 eV can be estimated (calculated for the intrinsic region between 280–360 K).

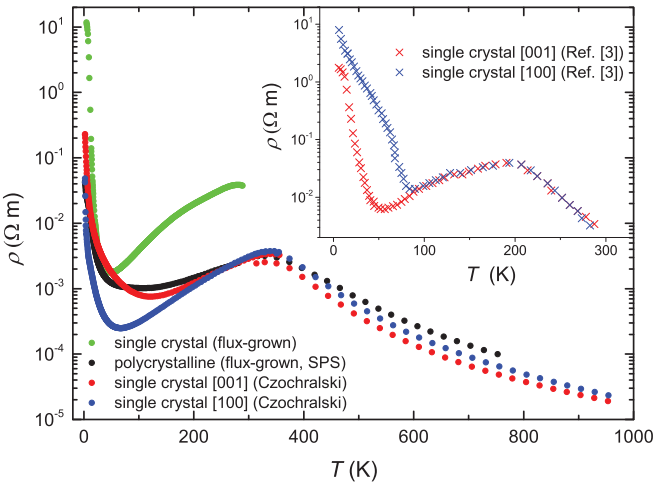

FIG. 3. (Color online) Electrical resistivity in dependence on the temperature for single-crystalline and polycrystalline $FeGa_3$ specimens. For comparison, single-crystal data [3] are included in the inset. Band-gap calculation with the Arrhenius law $\rho(T) = \exp(Eg/2k_BT)$ gives energy gaps of 0.38–0.51 eV.

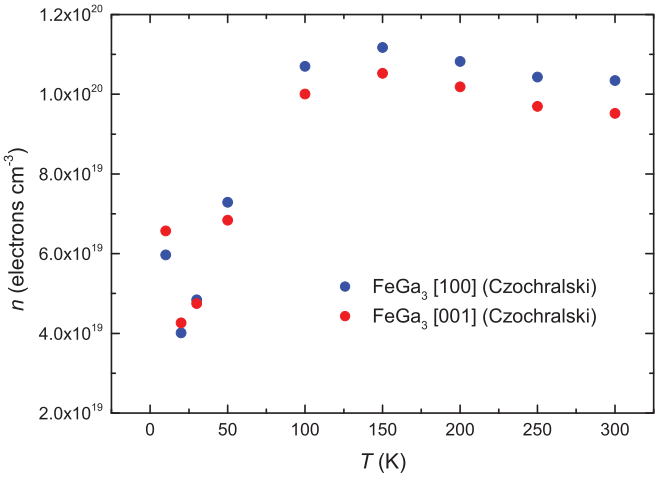

FIG. 4. (Color online) Charge carrier concentration n as a function of temperature for the oriented $FeGa_3$ single crystals (Czochralski method).

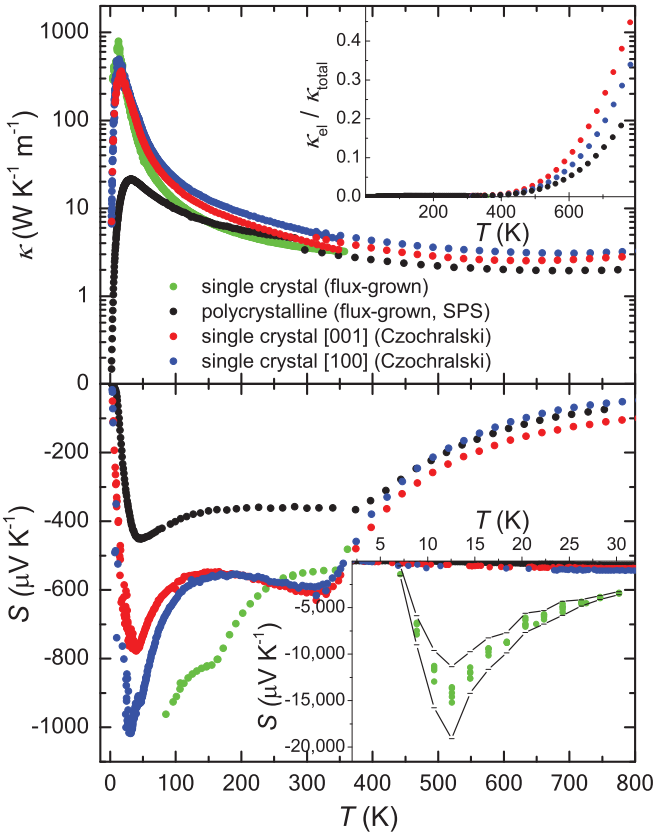

FIG. 5. (Color online) Top: Temperature dependence of the thermal conductivity for $FeGa_3$ specimens. The inset represents the contribution of the electronic part to the total thermal conductivity estimated with the Wiedemann-Franz law $\kappa_{el} = \rho\, L_0\, T$. Bottom: Seebeck coefficient of $FeGa_3$ specimens depending on the temperature. The inset shows high values for the flux-grown single crystal. The black solid curve in the inset represents the error for the Seebeck coefficient measurement, with $\Delta T = 10^{-3}$ K.

band at 2 K to be causing the minimum in the carrier concentration.

The temperature dependence of the thermal conductivity is plotted in Fig. 5(a). Remarkably huge peaks are observed for all single crystals in the temperature range from 13–16 K. Maximum values of ≈350 W K^{-1} m^{-1} for the single crystal (Czochralski method) with heat flow along the [001] direction, ≈500 W K^{-1} m^{-1} for the single crystal (Czochralski method) along the [100] direction and ≈800 W K^{-1} m^{-1} for the unoriented single crystal (flux grown) are observed, which are in contrast to previously published data (≈17.5 W K^{-1} m^{-1}) on oriented single crystals [3]. Due to the presence of grain boundaries in polycrystalline $FeGa_3$, which act as additional scatterers for phonons, the peak collapses yielding values of only ≈30 W K^{-1} m^{-1} at 21 K. At high temperatures, the thermal conductivity for the single-crystalline samples differs only slightly. No significant anisotropy in thermal conduction for $FeGa_3$ is observed over the whole temperature range. As expected, the polycrystalline material shows the lowest thermal conductivity among all investigated samples at high temperatures, being consistent to already published data [20]. The inset of Fig. 5(a) shows the electronic contribution to the total thermal conductivity estimated via the Wiedemann-Franz law $\kappa_{el} = \rho\, L_0 T$, where $L_0 = 2.45 \times 10^{-8}$ W Ω K^{-2} is the Lorenz number. Below 400 K, the total thermal conductivity is mainly determined by the lattice thermal conductivity, having nearly no contribution from the electronic part.

The results of the thermopower measurements are depicted in Fig. 5(b). In general, *n*-type behavior with electrons as majority carriers is observed over the whole temperature range, which is in contrast to the isostructural compounds $RuIn_3$ [40] and $RuGa_3$ [41], where a crossover behavior from *n* to *p* type is observed above room temperature. This is in line with the observed small Fe excess in our synthesized samples (see Table I).[2] At high temperatures, above 400 K similar behavior is observed for all samples independent from the crystallographic orientation. Below 400 K, distinct differences in absolute values are observed. The polycrystalline specimen with the highest defect concentration (e.g., grain boundaries) exhibits the lowest minimum Seebeck coefficient, comparable to published data [20,42]. The slight anisotropy is presumably electronically driven with an intersection point of the [100] and [001] curves around 200–250 K, as already observed in the electrical resistivity. Analogous to the sequence of the phonon peaks in the thermal conductivity, maximum thermopower values of −750 μV K^{-1} (single crystal via Czochralski method in the [001] direction) and −1000 μV K^{-1} (single crystal via Czochralski method in the [100] direction) appear. The inset of Fig. 5(b) shows the maximum thermopower value in the order of −16 000 μV K^{-1} measured for the unoriented single crystal (flux grown). Although the low-temperature maximum in the thermopower occurs at the same temperature (≈12 K) for all single-crystalline samples, the magnitude of *S* for the flux-grown crystal is 16–20 times larger than of the Czochralski single crystals. One main reason for this feature is the nonstandardized nature of the thermal gradient arising from the length difference between the samples: ⩽6 mm (flux grown) versus 8 mm (Czochralski). The obtained values of thermopower are comparable to published data on single crystals of intermetallic $CrSb_2$ [14] or $FeSb_2$ [5], but differ significantly to orientation-dependent measurements on $FeGa_3$ [3]. The authors of Ref. [3] report gallium inclusions of up to 3% in their single-crystalline samples, which could explain the difference between their data and our experimental thermopower.

The enhancement of thermopower at low temperatures in certain narrow-band-gap semiconductors has been shown to arise from increased electron-electron correlations, i.e., correlated semiconductors such as Kondo insulators. Specifically, for iron-based semiconductors such as FeSi and $FeSb_2$, large Seebeck coefficients at low temperatures (+500 μV K^{-1} at 50 K in FeSi [1], −45 000 μV K^{-1} at 10 K in $FeSb_2$ [4]) have been reported. This feature has been argued to arise due to the presence of strong electronic correlations in these two systems [6,43]. Although no static magnetic ordering has been observed in pure $FeGa_3$ until now,

[2]According to our DFT calculations, Fe carries a small negative charge.

weak ferromagnetic order has been observed [25] for the Ge-doped $FeGa_{3-x}Ge_x$ with $x = 0.13$ and weakly coupled local moments have been observed for Co-doped $Fe_{1-x}Co_xGa_3$ with $x = 0.05$ [44]. These attributes in $FeGa_3$ are also similar to FeSi and $FeSb_2$ where no static magnetic order is observed in the pure compounds, but ferromagnetic metallic states are discerned in $FeSi_{0.75}Ge_{0.25}$, $FeSb_{2-x}Te_x$, and $Fe_{1-x}Co_xSb_2$ [45–47].

C. DFT calculations

Previously, two works have addressed the eventuality of strong electronic correlations in $FeGa_3$ using DFT based calculations, but resulted in contradictory scenarios with one paper suggesting the presence of strong electronic correlations in the Fe 3*d* orbital [22], while the other refutes this scenario [48]. In both these papers, the authors only consider the band structure of nonmagnetic or magnetic $FeGa_3$, but not the band-structure-derived thermoelectric coefficients. Calculation of Seebeck coefficients involves the calculation of the band velocities, which are quite sensitive to the underlying band dispersions. Since there are no other additional parameters involved in the calculation of the Seebeck coefficients, the results are directly comparable to the experimental measurements, thus this could be used to identify the presence of strong correlations in $FeGa_3$. To that end, we have first calculated the nonmagnetic LDA density of states for $FeGa_3$ and the results are collected in Fig. 6. Consistent with previous calculations as well as our experiments, we obtain a semiconductor with a band gap of ≈0.52 eV. The valence and conduction band edges of $FeGa_3$ are derived primarily from Fe *d* states with only a small mixing of Ga. This feature is more clearly visible in the site-projected DOS in Fig. 6. Note the large difference in the *y*-axis values between Fe and Ga site-projected DOS. The valence band maximum is comprised mainly of Fe-$3d_{x^2-y^2}$ orbital character, while the conduction band minimum consists mainly of Fe-$3d_{3z^2-r^2}$ orbital character. There are sharp peaklike features in the DOS on either side of the Fermi level arising from flat bands. These sharp features are conducive for enhanced thermoelectric properties [49,50].

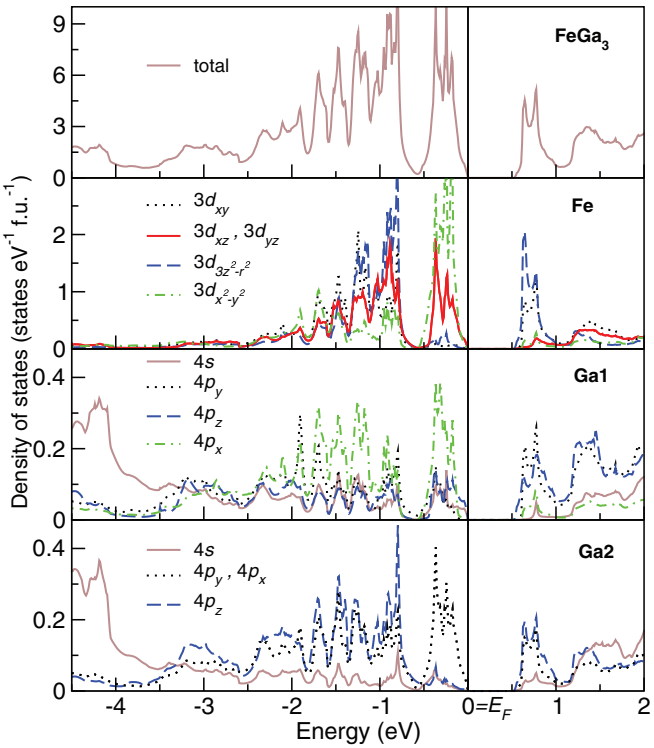

FIG. 6. (Color online) Nonmagnetic total and site-projected electronic density of states of $FeGa_3$.

As mentioned previously, although no magnetism has been observed for $FeGa_3$ in experiments, recently there has been some discussion about the presence of strong Coulomb correlations emerging from the narrow 3*d* bands of this semiconducting system using DFT based calculations. Using LSDA + *U* with FLL double counting scheme, a structure wherein the nearest-neighbor Fe sites are coupled antiferromagnetically with local moments on Fe of the order of $0.6\mu_B$ was found to be stable [22]. Additionally, a semiconducting gap of the order of 0.5 eV was obtained, similar to the experiments. To the contrary, using an optimized double counting scheme (screened by the Yukawa screening length λ) no magnetic moment on the iron ions was obtained [48]. Recently, another DFT work discusses the possibility of itinerant magnetism for both Ge (on the Ga site) and Co (on the Fe site) doped systems [26]. Itinerant Stoner ferromagnetism for the doped systems was readily obtained without invoking the need for preexisting moments in the parent semiconducting state, as well as without the need for correlation terms. Furthermore, the Seebeck coefficients were calculated as a function of doping, though only for the nonmagnetic ground state. In our work, we calculate the Seebeck coefficients of $FeGa_3$ for both the uncorrelated (LDA) and correlated (LSDA + *U*) scenarios to shed more light on the proceeding discussions. Collected in Fig. 7 are the results of the LSDA + *U* calculation (with FLL double counting scheme) for $U = 2$ eV, with a Hund's exchange $J = 0.625$ eV. The magnetic pattern used for this calculation is similar to that proposed in Ref. [22] with the two nearest Fe neighbors ordering antiferromagnetically (AFM). Surprisingly, the resulting AFM LSDA + *U* band

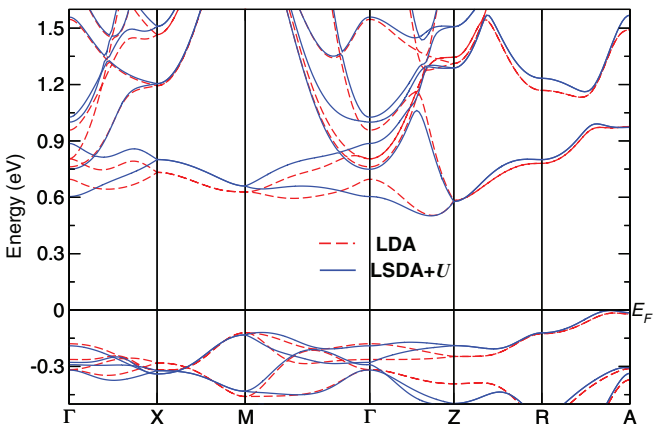

FIG. 7. (Color online) Comparison of the nonmagnetic LDA and the AFM LSDA + *U* band structures of $FeGa_3$. The nearest-neighbor Fe atoms are ordered antiferromagnetically in the LSDA + *U* calculation. A *U* value of 2 eV and a *J* value of 0.625 eV were used.

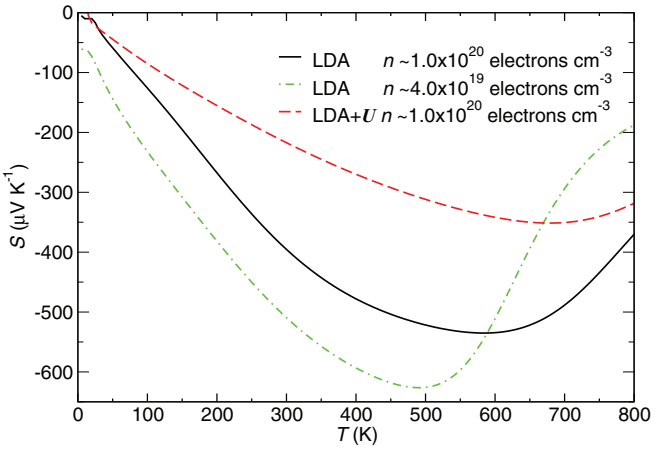

FIG. 8. (Color online) Calculated thermopower as a function of temperature for $FeGa_3$ for the two scenarios: LDA (nonmagnetic) and LSDA + U (antiferromagnetic, $U = 2$ eV). There is a significant difference in the calculated thermopower between LDA and LSDA + U, with the LDA curve being more in accordance with the experimentally measured thermopower.

structure close to the Fermi edge, including the size of the semiconducting gap is quite similar to that of the nonmagnetic LDA calculations. Moving away from the Fermi edge, we observe some differences between the LDA and LSDA + U bands in both the valence and conduction channels. These small differences could in turn alter the transport coefficients since they depend on the band velocities. Significant changes in the calculated Seebeck coefficients between LDA and LSDA + U calculations could provide an alternative view for identifying the presence or absence of magnetism and correlations (described in a mean field manner) in $FeGa_3$.

To that end, we have calculated the transport coefficients using the semiclassical Boltzmann theory. The similarity of the band gaps between LDA and AFM LSDA + U calculations permits a direct comparison between the two scenarios.[3] Collected in Fig. 8 are calculated data of the Seebeck coefficient as a function of temperature within LDA and LSDA + U for a carrier concentration $n \approx 1.0 \times 10^{20}$ electrons cm^{-3}, obtained from Hall effect measurements for a temperature range 100–300 K. The low-temperature enhancement in the Seebeck coefficient observed in the experiments around 20 K is not observed in either of the calculated curves. Decreasing the carrier concentration to $n \approx 4.0 \times 10^{19}$ electrons cm^{-3} also does not produce the low-temperature feature. The Seebeck coefficient increases monotonically up to 500 K for LDA and up to 700 K for LSDA + U, after which it starts to decrease. Above 150 K, the absolute values and the shape of S within LDA are more in accordance with the experimental observations and is larger than within LSDA + U by a factor of 2. Although the low-temperature feature is absent in our calculations, we can nevertheless infer that strong correlations, treated in a mean field manner, do not improve the description of the Seebeck coefficient in $FeGa_3$. More sophisticated calculations that treat Coulomb correlation U beyond a mean field approximation are necessary to obtain a more in-depth understanding of the role of correlations in $FeGa_3$ [51,52].

D. Heat-capacity and susceptibility measurements

We proceed to investigate the likelihood of a phase transition as a source for the low-temperature features in S and κ. To this end, we have measured the heat capacity and magnetic susceptibility for $FeGa_3$. The results of the heat-capacity measurement is collected in Fig. 9(a). The zero-field measurement does not show any jumps or kinks over the entire temperature range. Moreover, the data for 9 T

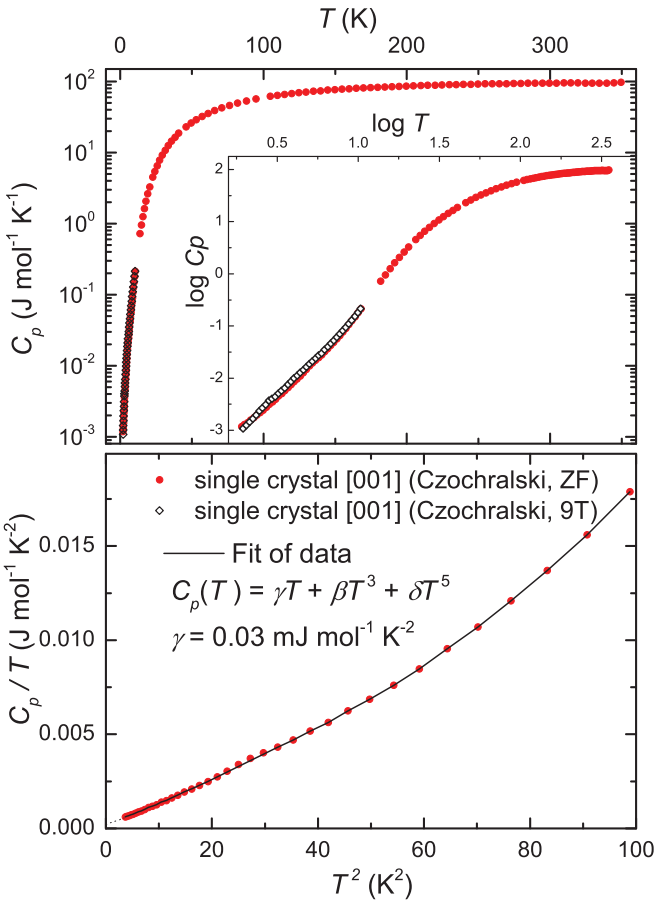

FIG. 9. (Color online) Top: Magnetic field dependence of the specific heat for a $FeGa_3$ single crystal (Czochralski method) oriented along [001] in zero field (ZF) and high field ($H = 9$ T). The inset shows a log-log plot. Bottom: Specific-heat data below 10 K in a C_p/T vs T^2 representation resulting in a Sommerfeld coefficient of $\gamma = 0.03$ mJ mol^{-1} K^{-1}.

[3]We make a note about plotting the experimental and calculated Seebeck coefficients in separate plots: In DFT, it is instructive to calculate the Seebeck coefficient for a fixed carrier concentration, while in reality the carrier concentration may vary as a function of temperature during experimental measurements (see Fig. 4). Hence, a combined plot of the experimental and calculated Seebeck coefficients would be misleading. For cases where the carrier concentration is temperature dependent, comparison between experiment and calculation is more qualitative than quantitative.

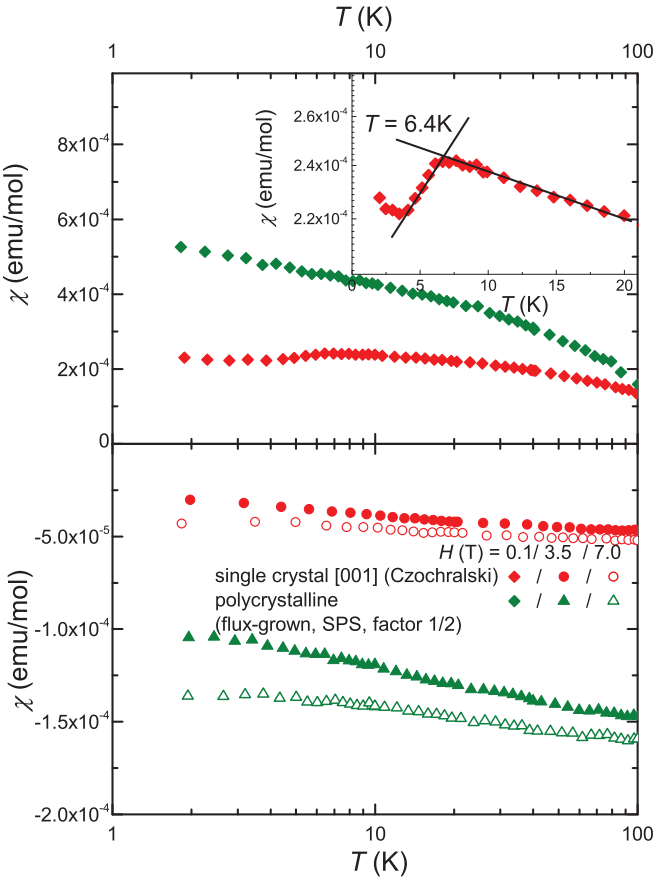

FIG. 10. (Color online) Top: Temperature dependence of magnetic susceptibility for $FeGa_3$ single crystal (Czochralski method) oriented along [001] and powder made of the single crystal (flux grown), which was additionally washed with hydrochloric acid in (top) low external field of $H = 0.1$ T and (bottom) high external fields of 3.5 and 7.0 T. The inset in the upper panel shows the magnification of temperatures below 20 K.

and low temperatures are also coinciding with the zero-field data. This implies that there are no structural phase transitions in $FeGa_3$. The value of the electronic specific-heat coefficient γ is obtained by plotting C_p/T versus T^2 [Fig. 9(b)] and fitting the data to $C_p = \gamma T + \beta T^3 + \delta T^5$. We obtained a better fit when including the T^5 term, which is associated to both the higher-order terms of the Fourier series of a harmonic oscillator and as well as to anharmonic terms [53]. This results in $\gamma = 0.03$ mJ mol^{-1} K^{-2}, close to zero as expected for a semiconductor and consistent with previously published values [3,25]. The Sommerfeld constant γ in the electronic specific heat can be compared to the bare value γ_b determined from the bare reference density of states at the Fermi level $N(0)$ [$\gamma_b = \pi^2 k_B^2 N(0)/3 = 2.359N(0)$], where $N(0)$ is in states/(eV f.u.) and γ_b is in mJ mol^{-1} K^{-2}. From Hall effect measurements, for a carrier concentration of $n \approx 1.0 \times 10^{20}$ electrons cm^{-3} (100–300 K) and $n \approx 4.0 \times 10^{19}$ electrons cm^{-3} (<100 K), we use the $N(0)$ from our band-structure calculations and obtain $\gamma_b = 0.06$ mJ mol^{-1} K^{-2} and 0.01 mJ mol^{-1} K^{-2}, respectively, consistent with the experimental observation.

The temperature dependence of the magnetic susceptibility measured at various fields is displayed in Fig. 10. For fields of 3.5 and 7 T, the measured $\chi(T)$ for the [001]-oriented single crystal (Czochralski method) is negative for the entire temperature range up to 300 K and diamagnetic. The slight upturn at low temperatures originates from the tiny amounts of Fe impurities in the system. This fact is clearly visible in the low-field 0.1-T data where the susceptibility values at low temperatures are positive. For the [001]-oriented single crystal (Czochralski method), in 0.1-T field, we observe a sharp downward turn around 6.4 K. We were able to correlate this feature to the onset of superconductivity from tiny amounts of Ga inclusions in thin film form ($T_c = 7.6$ K) [54]. The gallium inclusions were removed by grinding the sample and washing it with diluted hydrochloric acid (H_2O:HCl = 1:1). The susceptibility measurements on the so-obtained polycrystalline sample did not show any downturn at low temperatures. Consistent with the heat-capacity measurements, we do not observe any other anomalous features in $\chi(T)$ that could point towards the possibility of a magnetic phase transition.

E. Phonon-drag mechanism

Having excluded both structural and magnetic phase transition at low temperatures, and as well as the presence of strong electronic correlations in $FeGa_3$, another possible explanation for the unusually strong signal below 20 K in the thermopower and the thermal conductivity is a phonon-drag mechanism. The peaks in the thermal conductivity and Seebeck coefficient for all the single-crystalline samples always occur at the same temperature, ≈20 K. Moreover, the trend in the peak intensity between κ and S is similar: $\kappa_{\text{polycrystalline}} < \kappa_{[001]} < \kappa_{[100]} < \kappa_{\text{unoriented}}$ and $S_{\text{polycrystalline}} < S_{[001]} < S_{[100]} < S_{\text{unoriented}}$. The peak in the low-temperature thermal conductivity for the flux-grown single crystal is more than 25 times larger than for the polycrystalline sample. Similarly, the peak in the Seebeck coefficients for the flux-grown single crystal is also larger than the powder sample (prepared from the flux-grown sample) by a factor of ≈30. Such features have been observed in other semiconductors including single crystals of Ge [55], Si [56], and $CrSb_2$ [14] nanocomposite $FeSb_2$ [8], reduced TiO_2 [57,58], ultrathin films of $FeSi_2$ and $MnSi_{1.7}/FeSi_2$ [59], which have subsequently been demonstrated to arise from phonon-drag effects. Phonon drag can be defined as the effect arising from a preferential scattering of the charge carriers by the phonons in the direction of the flow (i.e., the drag on the charge carriers exerted by the phonons streaming from hot to cold end in thermal conduction) and mostly evidenced at low temperatures. With increasing temperatures, the magnitude of the phonon-drag influenced Seebeck coefficient decreases rapidly. This is due to the reduced relaxation time for the long-wavelength phonons, which interact with the electrons/holes, as a result of the increase in the carrier concentration. Due to this electron-phonon coupling at reduced temperatures, the Seebeck coefficient can now be written as a sum of the conventional electron-diffusion part S_d and another term arising from the phonon-electron interaction S_p, the so-called phonon-drag contribution

$$S = S_d + S_p.$$

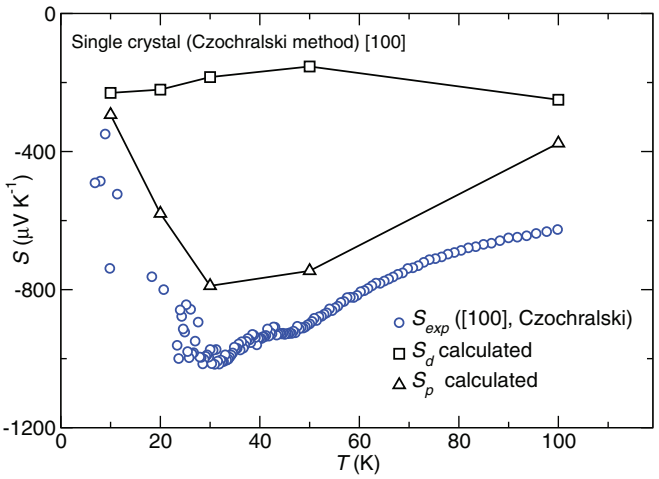

FIG. 11. (Color online) Comparison of the measured Seebeck coefficient with the calculated values of the diffusive (S_d) and phonon-drag (S_p) parts as a function of temperature for a single crystal of $FeGa_3$ (Czochralski method) along [100]. The S_p term dominates the low-temperature regime, indicative of a significant phonon-drag effect in this system.

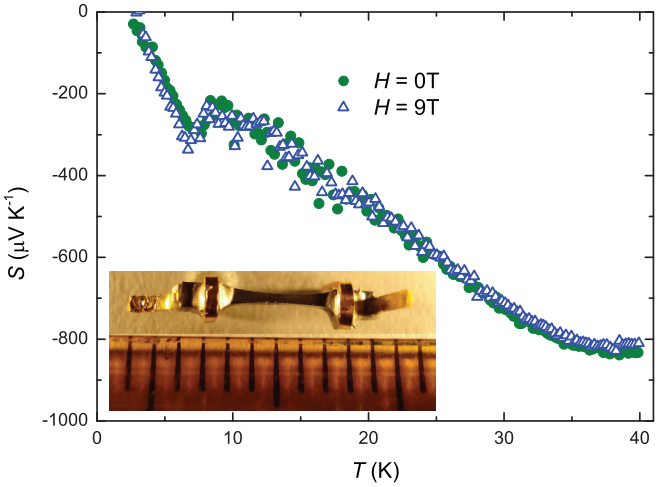

FIG. 12. (Color online) Temperature dependence of the Seebeck coefficient for a single crystal of $FeGa_3$ (Czochralski method) oriented along the [100] direction, measured both at 0- and 9-T magnetic fields. The magnetic field was applied along [100], parallel to the crystallographic orientation. The lack of significant changes in S at 0 and 9 T supports the nonelectronic origin of the colossal low-temperature values and thus can be attributed to phonon-drag mechanism. The slight difference in the thermopower data compared to Fig. 5 is due to the change in the shape of the sample to improve the heat flow (see inset).

Although an accurate quantitative calculation for a phonon-drag contribution is difficult to obtain, one can realize an estimate by calculating the electron-diffusion part and subtracting it from the measured total Seebeck coefficient. For a semiconductor with a complex band structure and whose spin-orbit splitting is negligible ($\ll k_B T$), the electron-diffusion part as suggested by Herring [60] can be written as

$$S_d = \mp 86.2\left[\ln\frac{4.70\times10^{15}}{n} + \frac{3}{2}\ln\frac{m^*}{m} + \frac{|\Delta\epsilon_T|}{k_B T} + \frac{3}{2}\ln T\right],$$

where the minus and plus signs are for the n- and p-type carriers, respectively, n is the charge carrier density denoted in cm^{-3}, m and m^* are the bare and inertial effective masses of the electron, respectively, $|\Delta\epsilon_T|$ refers to the average energy of the transported electrons relative to the band edge, and k_B is the Boltzmann constant. Usually, $|\Delta\epsilon_T|$ is of the order of $k_B T$, and in the diffusive limit (i.e., lattice scattering by phonons of long wavelength), Herring [60] proposes an additional approximation of $|\Delta\epsilon_T| = \frac{5}{2} + r$ with $r = -\frac{1}{2}$. Figure 11 displays the S_d values obtained from the above equation using $m^* = m$ and n from Hall resistivity measurements (Fig. 4). Subsequently, S_p was calculated by subtracting S_d from the total S. We note that the S_p contribution to the total S is dominant over the electron-diffusive S_d term in the low-temperature regime and thus indicative of a significant phonon-drag effect in $FeGa_3$.

Another method to eliminate the possibility of an electronic origin to the colossal low-temperature Seebeck coefficient is to measure in high magnetic fields [14]. If the system is dominated by the phonon-drag mechanism, only a small response in the magnetic field is expected. To confirm this scenario, we measured the Seebeck coefficient for a [100]-oriented $FeGa_3$ single crystal (Czochralski method) at 9 T and the results are displayed in Fig. 12. The lack of difference between the 0- and 9-T data up to 40 K is apparent and upholds the nonelectronic origin of the pronounced peak in the Seebeck coefficient.

IV. SUMMARY

We have synthesized single-crystalline and polycrystalline samples of the narrow-band-gap semiconductor $FeGa_3$. A band gap of ≈0.5 eV is obtained from electrical resistivity measurements. Systematic investigation of the thermoelectric properties of the single-crystalline and polycrystalline samples reveals pronounced peaks around 20 K in the thermal conductivity (400–800 W K^{-1} m^{-1}) and the Seebeck coefficient (in the order of $-16\,000$ μV K^{-1}). Such large values have previously not been reported for $FeGa_3$. To identify the origin of the low-temperature enhancement, we investigated various possibilities. DFT based band-structure calculations and subsequent modeling of the Seebeck coefficient using semiclassical Boltzmann transport theory yielded a Seebeck coefficient of the same order as the experiment above 300 K with LDA. Inclusion of strong electronic correlations arising from the narrow Fe-d bands treated in a mean field manner (LSDA + U) does not improve this comparison, rendering strong correlations as an explanation for the low-temperature enhancement in Seebeck unlikely. Heat-capacity and magnetic susceptibility measurements under different applied magnetic fields do not show any kinks or jumps around 20 K and thus exclude a magnetic or structural phase transition as a reason for the low-temperature peak in the Seebeck coefficient. Comparing the trend in the Seebeck coefficient and thermal conductivity among the various samples, and based on estimates of the phonon-drag

contribution to the Seebeck coefficient and the negligible response in a high magnetic field, we conclude that the low-temperature enhancements in $FeGa_3$ are due to a phonon-drag effect.

Note added. Recently, we became aware of another work on the binary $FeGa_3$ and the hole-doped variants $Fe_{1-x}Mn_xGa_3$ and $FeGa_{3-y}Zn_y$ [61]. In contrast to our work which focuses on the anomalous thermoelectric properties of $FeGa_3$ at very low temperatures (below 50 K), Gamża *et al.* focus on the magnetic properties of both the binary and the hole-doped variants up to very high temperatures (≈800 K) [61]. Comparison of the lattice parameters, electrical resistivity, and thermodynamic measurements of our flux-grown single crystals with that of Gamża *et al.* [61] demonstrates the similarity between our samples. A fit to the Arrhenius law for the intrinsic region (>350 K) of the resistivity gave a band gap of 0.5 eV in our work for the single crystals grown using the Czochralski method, while Gamża *et al.* obtain a value of 0.4 eV for their flux-grown samples [61]. Signatures of a complex magnetic ordering are presented based on neutron diffraction measurements. In contrast, LDA+DMFT (dynamical mean field theory) calculations do not show any hint of long-range antiferromagnetic ordering [61]. However, in our work, applying LSDA + U as a simple mean field treatment of electronic correlations, we could stabilize a simple AFM order. Nevertheless, this approximation did not improve the description of the thermopower.[4]

ACKNOWLEDGMENTS

The authors acknowledge x-ray powder diffraction measurements and WDXS analysis by the competence groups Structure and Metallography at the MPI CPfS. We also thank R. Koban for help with physical properties measurements. D.K., H.R., and Yu.G. acknowledge funding by the Deutsche Forschungsgemeinschaft (DFG) within Schwerpunktprogramm (SPP) 1386.

[4]The neutron diffraction pattern of Gamża *et al.* [61] shows a complex magnetic ordering in $FeGa_3$. Using LSDA + U, we have stabilized only a simple AFM order wherein nearest-neighbor Fe sites are ordered antiferromagnetically. The discrepancy between the measured and calculated Seebeck coefficient could then arise for two possible reasons: the treatment of correlations in a mean field manner is insufficient or the simple AFM order we consider is not a good approximation for the complex magnetic order observed in the experiments.

[1] B. C. Sales, E. C. Jones, B. C. Chakoumakos, J. A. Fernandez-Baca, H. E. Harmon, J. W. Sharp, and E. H. Volckmann, Phys. Rev. B **50**, 8207 (1994).
[2] C. Petrovic, J. W. Kim, S. L. Bud'ko, A. I. Goldman, P. Canfield, W. Choe, and G. J. Miller, Phys. Rev. B **67**, 155205 (2003).
[3] Y. Hadano, S. Narazu, M. A. Avila, T. Onimaru, and T. Takabatake, J. Phys. Soc. Jpn. **78**, 013702 (2009).
[4] A. Bentien, S. Johnsen, G. K. H. Madsen, B. B. Iversen, and F. Steglich, Europhys. Lett. **80**, 17008 (2007).
[5] P. Sun, N. Oeschler, S. Johnsen, B. B. Iversen, and F. Steglich, Dalton Trans. **39** , 1012 (2009).
[6] P. Sun, M. Søndergaard, B. B. Iversen, and F. Steglich, Ann. Phys. (Berlin) **523**, 612 (2011).
[7] H. Takahashi, R. Okazaki, Y. Yasui, and I. Terasaki, Phys. Rev. B **84**, 205215 (2011).
[8] M. Pokharel, H. Zhao, K. Lukas, Z. Ren, C. Opeil, and B. Mihaila, Mater. Res. Soc. Commun. **3**, 31 (2013).
[9] J. M. Tomczak, K. Haule, and G. Kotliar, Proc. Natl. Acad. Sci. USA **109**, 3243 (2012).
[10] J. H. Wijngaard, C. Haas, and R. A. de Groot, Phys. Rev. B **45**, 5395 (1992).
[11] M. A. McGuire, A. D. Christianson, A. S. Sefat, B. C. Sales, M. D. Lumsden, R. Jin, E. A. Payzant, D. Mandrus, Y. Luan, V. Keppens, V. Varadarajan, J. W. Brill, R. P. Hermann, M. T. Sougrati, F. Grandjean, and G. J. Long, Phys. Rev. B **78**, 094517 (2008).
[12] T. Souma, G. Nakamoto, and M. Kurisu, J. Alloys Compd. **340**, 275 (2002).
[13] B. Büchner, M. Cramm, M. Braden, W. Braunisch, O. Hoffels, W. Schnelle, R. Müller, A. Freimuth, W. Schlabitz, G. Heger, D. Khomskii, and D. Wohlleben, Europhys. Lett. **21**, 953 (1993).
[14] B. C. Sales, A. F. May, M. A. McGuire, M. B. Stone, D. J. Singh, and D. Mandrus, Phys. Rev. B **86**, 235136 (2012).
[15] K. Schubert, H. L. Lukas, H.-G. Meissner, and S. Bhan, Z. Metallkd. **50**, 534 (1959).
[16] K. Schubert, H. Breimer, R. Göhle, H. L. Lukas, H.-G. Meissner, and E. Stolz, Naturwissenschaften **45**, 360 (1958).
[17] C. Dasarathy and W. Hume-Rothery, Proc. R. Soc. A **286**, 141 (1965).
[18] S. S. Lu and C.-K. Liang, Acta Phys. Sin. **21**, 849 (1965).
[19] U. Häussermann, M. Boström, P. Viklund, Ö. Rapp, and T. Björnängen, J. Solid State Chem. **165**, 94 (2002).
[20] Y. Amagai, A. Yamamoto, T. Iida, and Y. Takanashi, J. Appl. Phys. **96**, 5644 (2004).
[21] N. Tsujii, H. Yamaoka, M. Matsunami, R. Eguchi, Y. Ishida, Y. Senba, H. Ohashi, S. Shin, T. Furubayashi, H. Abe, and H. Kitazawa, J. Phys. Soc. Jpn. **77**, 024705 (2008).
[22] Z. P. Yin and W. E. Pickett, Phys. Rev. B **82**, 155202 (2010).
[23] V. G. Storchak, J. H. Brewer, R. L. Lichti, R. Hu, and C. Petrovic, J. Phys.: Condens. Matter **24**, 185601 (2012).
[24] M. Arita, K. Shimada, Y. Utsumi, O. Morimoto, H. Sato, H. Namatame, M. Taniguchi, Y. Hadano, and T. Takabatake, Phys. Rev. B **83**, 245116 (2011).
[25] K. Umeo, Y. Hadano, S. Narazu, T. Onimaru, M. A. Avila, and T. Takabatake, Phys. Rev. B **86**, 144421 (2012).
[26] D. J. Singh, Phys. Rev. B **88**, 064422 (2013).
[27] P. Gille and B. Bauer, Cryst. Res. Technol. **43**, 1161 (2008).
[28] K. Koepernik and H. Eschrig, Phys. Rev. B **59**, 1743 (1999).
[29] J. P. Perdew and Y. Wang, Phys. Rev. B **45**, 13244 (1992).
[30] J. M. Ziman, *Electrons and Phonons* (Oxford University Press, New York, 2001).

[31] W. Jones and N. H. March, *Theoretical Solid State Physics* (Courier Dover, New York, 1985).
[32] G. K. H. Madsen, K. Schwarz, P. Blaha, and D. J. Singh, Phys. Rev. B **68**, 125212 (2003).
[33] G. K. H. Madsen and D. J. Singh, Comput. Phys. Commun. **175**, 67 (2006).
[34] S. Johnsen, A. Bentien, G. K. H. Madsen, B. B. Iversen, and M. Nygren, Chem. Mater. **18**, 4633 (2006).
[35] D. J. Singh and D. Kasinathan, J. Electron. Mater. **36**, 736 (2007).
[36] H. J. Xiang and D. J. Singh, Phys. Rev. B **76**, 195111 (2007).
[37] D. Kasinathan, M. Wagner, K. Koepernik, R. Cardoso-Gil, Y. Grin, and H. Rosner, Phys. Rev. B **85**, 035207 (2012).
[38] See Supplemental Material at http://link.aps.org/Supplemental/10.1103/PhysRevB.90.195206 for the XRD pattern.
[39] H. Fritzche, Phys. Rev. **99**, 406 (1955).
[40] M. Wagner, R. Cardoso-Gil, N. Oeschler, H. Rosner, and Y. Grin, J. Mater. Res. **26**, 1886 (2011).
[41] M. Wagner-Reetz, R. Cardoso-Gil, Yu. Prots, W. Schnelle, and Y. Grin, Sol. Stat. Sci. **32**, 56 (2014).
[42] N. Haldolaarachchige, A. B. Karki, W. A. Phelan, Y. M. Xiong, R. Jin, J. Y. Chan, S. Stadler, and D. P. Young, J. Appl. Phys. **109**, 103712 (2011).
[43] G. Aeppli and Z. Fisk, Comments Condens. Matter Phys. **16**, 155 (1992).
[44] E. M. Bittar, C. Capan, G. Seyfarth, P. G. Pagliuso, and Z. Fisk, J. Phys.: Conf. Ser. **200**, 012014 (2010).
[45] S. Yeo, S. Nakatsuji, A. D. Bianchi, P. Schlottmann, Z. Fisk, L. Balicas, P. A. Stampe, and R. J. Kennedy, Phys. Rev. Lett. **91**, 046401 (2003).
[46] R. Hu, V. F. Mitrović, and C. Petrovic, Phys. Rev. B **79**, 064510 (2009).
[47] R. Hu, V. F. Mitrović, and C. Petrovic, Phys. Rev. B **74**, 195130 (2006).
[48] J. M. Osorio-Guillén, Y. D. Larrauri-Pizarro, and G. M. Dalpian, Phys. Rev. B **86**, 235202 (2012).
[49] G. D. Mahan and J. O. Sofo, Proc. Natl. Acad. Sci. USA **93**, 7436 (1996).
[50] J. K. Freericks, D. O. Demchenko, A. V. Joura, and V. Zlatić, Phys. Rev. B **68**, 195120 (2003).
[51] C. Grenzebach, F. B. Anders, G. Czycholl, and T. Pruschke, Phys. Rev. B **74**, 195119 (2006).
[52] J. K. Freericks and V. Zaltić, Phys. Rev. B **64**, 245118 (2001).
[53] R. Pässler, AIP Advances **3**, 082108 (2013).
[54] G. Kieselmann, in *Ga Elements, Ga Films, Ga/X Junctions*, edited by R. Flükiger and W. Klose, Landolt-Börnstein-Group III Condensed Matter Vol. 21a (Springer, Berlin, 1985), pp. 249–258.
[55] T. H. Geballe and G. W. Hull, Phys. Rev. **94**, 1134 (1954).
[56] T. H. Geballe and G. W. Hull, Phys. Rev. **98**, 940 (1955).
[57] W. R. Thurber and J. H. Mante, Phys. Rev. **139**, A1655 (1965).
[58] J. Tang, W. Wang, G.-L. Zhao, and Q. Li, J. Phys.: Condens. Matter **21**, 205703 (2009).
[59] Q. R. Hou, B. F. Gu, Y. B. Chen, and Y. J. He, Mod. Phys. Lett. B **25**, 1829 (2011).
[60] C. Herring, Phys. Rev. **96**, 1163 (1954).
[61] M. B. Gamża, J. M. Tomczak, C. Brown, A. Puri, G. Kotliar, and M. C. Aronson, Phys. Rev. B **89**, 195102 (2014).